ASME 2012 5th Annual Dynamic Systems and Control Conference joint with the JSME 2012 11th Motion and Vibration Conference
DSCC2012-MOVIC2012
October 17-19, 2012, Fort Lauderdale, Florida, USA

DSCC2012-MOVIC2012-8649

NONINVASIVE BATTERY-HEALTH DIAGNOSTICS USING RETROSPECTIVE-COST IDENTIFICATION OF INACCESSIBLE SUBSYSTEMS

Anthony M. D'Amato
Department of Aerospace Engineering
The University of Michigan
Ann Arbor, Michigan 48109

Joel C. Forman
Tulga Ersal
Department of Mechanical Engineering
The University of Michigan
Ann Arbor, Michigan 48109

Asad A. Ali
Department of Aerospace Engineering
The University of Michigan
Ann Arbor, Michigan 48109

Jeffrey L. Stein
Huei Peng
Department of Mechanical Engineering
The University of Michigan
Ann Arbor, Michigan 48109

Dennis S. Bernstein*
Department of Aerospace Engineering
The University of Michigan
Ann Arbor, Michigan 48109
Email: dsbaero@umich.edu

ABSTRACT

Health management of Li-ion batteries depends on knowledge of certain battery internal dynamics (e.g., lithium consumption and film growth at the solid-electrolyte interface) whose inputs and outputs are not directly measurable with noninvasive methods. This presents a problem of identification of inaccessible subsystems. To address this problem, we apply the retrospective-cost subsystem identification (RCSI) method. As a first step, this paper presents a simulation-based study that assumes as the truth model of the battery an electrochemistry-based battery charge/discharge model of Doyle, Fuller, and Newman, and later augmented with a battery-health model by Ramadass. First, this truth model is used to generate the data needed for the identification study. Next, the film-growth component of the battery-health model is assumed to be unknown, and the identification of this inaccessible subsystem is performed using RCSI. The results show that the subsystem identification method can identify the film growth quite accurately when the chemical reactions leading to film growth are consequential.

INTRODUCTION

Due to their higher energy density compared to their lead-acid and nickel-metal-hydride counterparts, Lithium-ion (Li-ion) batteries have found a wide range of applications from handheld electronic devices to electrified vehicles. Understanding and optimally managing their health is critical for improving their reliability, durability, and cost.

Li-ion batteries have various degradation mechanisms depending on which combination of anode, cathode, electrolyte, and dopant chemistries are used. Provided the battery's minimum and maximum voltages are not exceeded, the predominant degradation mechanism in Li-ion batteries with lithium-iron-phosphate ($LiFePO_4$) cathodes is Solid-Electrolyte Interface (SEI) film formation in the anode (1). This mechanism affects battery State of Health (SoH) in two ways, namely, the film resists intercalation current, increasing internal resistance, and film creation consumes Li-ions, decreasing battery capacity. Film formation depends on how the battery is charged, discharged, and stored.

To control degradation, it is necessary to predict how charging, discharging, and storage patterns affect SoH and then modify these patterns subject to operating constraints and objectives. Noninvasive methods, such as methods based on equivalent-circuit models for capacity and power, have been used to correlate static parameters of SEI film thickness (2; 3; 4). However, these methods do not model the dynamics of film growth and thus do not allow the battery-management system to modify charging patterns based on predicted future health. On the other

*Address all correspondence to this author.

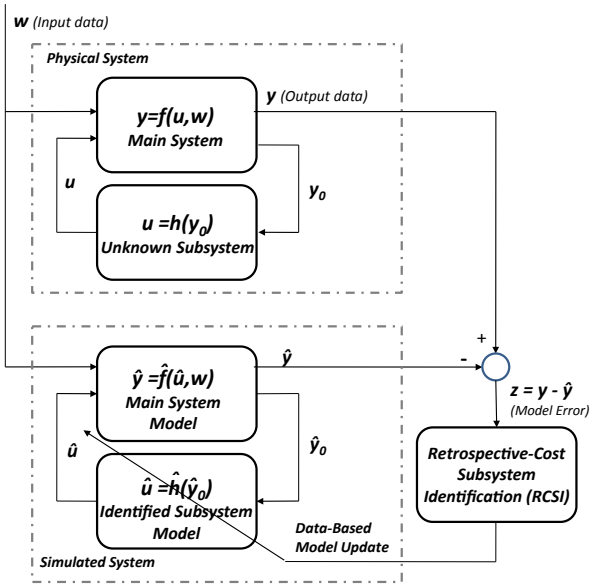

Figure 1. Identification of an unknown inaccessible subsystem whose input y_0 and output u are not measured. The only measured data are w and y.

hand, direct measurements of film growth require invasive methods that destroy the battery and are thus not applicable during the lifetime of the battery. Therefore, the goal of this paper is to use system identification to construct an empirical film-growth model as a noninvasive approach to battery-health diagnostics.

The dynamics of film growth constitute a subsystem of the overall battery model, and thus the goal is to identify the dynamics of the film-growth subsystem while taking advantage of a given model of the main battery subsystem. However, identification of the film-growth subsystem is challenging due to the fact that its inputs and outputs are not available from noninvasive measurements. In this case, we say that the subsystem is *inaccessible*. Figure 1 illustrates the subsystem identification problem, where the input y_0 and output u of the Unknown Subsystem are not measured.

To address the inaccessible subsystem identification problem, we apply *retrospective-cost subsystem identification* (RCSI) developed in (5; 6; 7; 8). The investigation of RCSI for noninvasive battery health diagnostics is motivated by the method's ability to estimate an inaccessible cooling submodel within an ionosphere-thermosphere model (9).

Figure 1 shows the RCSI framework. In the present paper we adopt a simulation-based approach and consider as the "Physical" System in Fig. 1 the Doyle-Fuller-Newman (DFN) battery model (10; 11) augmented with the Ramadass battery-health model (12) (DFN+R). The DFN+R model is considered as the "truth" model, with the DFN model together with the Li consumption component of the battery-health model as the Main System, and the film-growth component of the battery-health model as the Unknown Subsystem. This truth model is then used for a simulation-based demonstration of RCSI where the goal is to identify the film-growth portion of the battery-health dynamics. To do this, we first simulate the DFN+R battery model to obtain data for use in subsystem identification. Next, we remove the film-growth component of the battery-health model, treating it as unknown, and use the DFN model augmented with the Li consumption component of the battery-health model as the Main System Model for RCSI. Hence, in this paper, the Main System and Main System Model blocks shown in Fig. 1 are identical. We then apply RCSI to identify the film-growth subsystem model. For validation, we compare the output of the actual battery-health subsystem with the output of the battery-health subsystem model obtained from RCSI.

The rest of the paper is organized as follows. The *Battery Model* section gives an overview of the battery model used in this study. The RCSI method is reviewed in *Retrospective-Cost Sybsystem Identification* section. The *Numerical Simulation* section demonstrates the application of RCSI to the film-growth idetification problem. Conclusions are given in the final section.

BATTERY MODEL

Dynamics of Charging and Discharching

The DFN model is an electrochemical battery model that captures concentration and potential distributions across the width of the cell as well as concentration profiles in the porous electrodes of the anode and cathode. The model is described in (10; 11; 12). This section summarizes the model equations, which constitute a system of nonlinear partial differential algebraic equations.

As seen in Fig. 2, Li-ion battery cells consist of an anode, separator, and cathode sandwiched between current collectors. Both the anode and cathode are made of porous solid material immersed in an electrolyte solution. When the battery is fully charged, most of the Li-ions occupy interstitial sites on the solid material in the anode. As the battery discharges, the Li-ions leave these interstitial sites, entering the electrolyte solution. The Li-ions then migrate through the solution from the anode to the separator and then to the cathode. Eventually, the Li comes to rest at interstitial sites on the solid in the cathode. When a Li-ion leaves its interstitial site in the anode, an electron is freed to flow through the circuit producing useful work. When this electron reaches the cathode it causes a different Li-ion to bond with a cathode interstitial site. Charging the battery is the same process in reverse, except that the circuit provides energy rather than consumes it.

The DFN model captures local Li-ion concentrations and potentials using coupled partial differential equations (PDEs). The PDEs account for the linear diffusion of Li-ions in the electrolyte, spherical diffusion of Li-ions in the solid, and the spatially distributed electrochemical reactions driving them to transfer between the solution and the solid. The remainder of this section briefly outlines the mathematical equations behind these

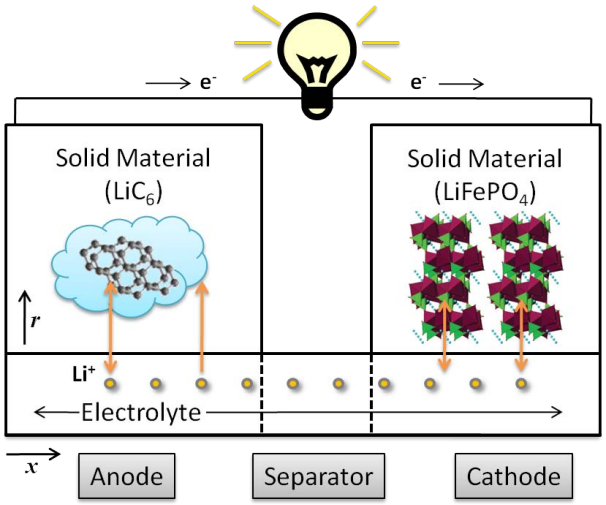

Figure 2. Li-ion cell schematic

phenomena.

The concentration $c_2(x,t)$ of Li-ions within the electrolyte is governed by Fick's law of linear diffusion combined with an intercalation current density term J transferring Li-ions between the solution and solid as modeled by

$$\varepsilon_2 \frac{\partial c_2}{\partial t} = \nabla(d_2^{eff} \nabla c_2) + \frac{1-t^+}{F} J. \tag{1}$$

The intercalation current density J also acts as an input to the dynamics of Li-ion diffusion within the solid. This diffusion occurs at every point in the anode and cathode and can be modeled using a spherical, radially symmetric diffusion law given by

$$\frac{\partial c_{1,j}}{\partial t} = \frac{D_{1,j}}{r^2} \frac{\partial}{\partial r} \left(r^2 \frac{\partial c_{1,j}}{\partial r} \right). \tag{2}$$

The total intercalation current density J equals the main intercalation reaction current density J_1 plus any additional intercalation current density J_s representing side reactions in the battery. The main intercalation reaction current density J_1 is driven by potential differences between the solid and electrolyte solution, and governed by the Butler-Volmer equation

$$J_1 = a_j i_{0,j} \left(e^{\frac{\alpha_{a,j} F}{RT} \eta_j} - e^{-\frac{\alpha_{a,j} F}{RT} \eta_j} \right), \tag{3}$$

where

$$i_{0,j} = k_j \left(c_{1,j}^{max} - c_{1,j}^S \right)^{\alpha_{a,j}} \left(c_{1,j}^S \right)^{\alpha_{c,j}} \left(c_2 \right)^{\alpha_{a,j}}. \tag{4}$$

The over-potentials in these equations equal the differences between the solid and solution potentials minus the reference potentials for the main intercalation reaction, which in turn depend on the local State of Charge (SoC) according to

$$\eta_p = \phi_1 - \phi_2 - u_{p,ref}, \tag{5}$$

$$\eta_n = \phi_1 - \phi_2 - u_{n,ref} - \frac{J}{a_n} R_{SEI}. \tag{6}$$

Since the potentials and over-potentials can change much faster than the Li-ion concentrations, they are assumed to respond instantaneously. The solid potential is governed by Ohm's law with a term governing the charge transfer due to intercalation as given by

$$\nabla \left(\sigma_j^{eff} \nabla \phi_{1,j} \right) - J = 0. \tag{7}$$

Similarly, the solution potential is governed by Ohm's law, the intercalation current density, and the charge carried by the ions in solution as modeled by

$$\nabla \left(\kappa^{eff} \nabla \phi_2 \right) + J + \nabla \left(\kappa_D \nabla \ln(c_2) \right) = 0. \tag{8}$$

This system of equations governs the dynamics of charging and discharging in the Li-ion cell. When the DFN model is discretized, it becomes a system of Differential Algebraic Equations (DAEs), where the differential equations govern the diffusion dynamics and the algebraic equations constrain the potentials and intercalation current.

Battery-Health Submodel

The truth model for battery health used later in this paper is based on a side reaction that simultaneously increases the anode SEI resistance and consumes cyclable Li-ions (12). This side reaction is given by

$$\eta_s = \phi_1 - \phi_2 - u_{sd,ref} - \frac{J}{a_n} R_{\text{film}}, \tag{9}$$

$$J_s = -i_{0s} a_n e^{-\frac{\alpha F}{RT} \eta_s}. \tag{10}$$

The side reaction creates a resistive film at a rate proportional to the side reaction current density, that is,

$$\frac{\partial \delta_{\text{film}}}{\partial t} = -\frac{J_s M_p}{a_n \rho_p F} \tag{11}$$

The resistive film adds to the internal resistance of the anode, thereby negatively affecting battery performance as modeled by

$$R_{\text{film}} = R_{SEI} + \frac{\delta_{\text{film}}}{K_p}. \tag{12}$$

Additionally, this model consumes cyclable Li-ions through the intercalation side current J_s and (1), resulting in capacity fade.

For subsystem identification, this health model is separated into two components, namely, film growth and Li-ion consumption. The film growth portion is identified by RCSI, whereas the Li-ion consumption piece is assumed to be part of the main model. Specifically, J_s is computed from the main model using (10), which is taken as an input to the RCSI algorithm. However, (11) and (12) are unknown to the RCSI algorithm; it is RCSI's task to create a model that represents these equations based on the simulated data it receives.

RETROSPECTIVE-COST SUBSYSTEM IDENTIFICATION

This section describes the RCSI method that is used to identify the inaccessible film-growth subsystem of the battery.

Retrospective Surrogate Cost-Based Signal Construction

Consider the MIMO discrete-time system

$$x(k+1) = f(x(k)) + g_u(u(k)) + g_{k,w}(w(k)), \tag{13}$$
$$y(k) = h_k(x(k)), \tag{14}$$
$$y_0(k) = h_0(x(k)), \tag{15}$$

where $f(\cdot)$, $g_u(\cdot)$ and $g_{k,w}(\cdot)$ are the battery dynamics (1)–(8), $x(k) \in \mathbb{R}^n$ is the internal battery state, $y(k) \in \mathbb{R}^{l_y}$ is either I or V depending on cycle, $y_0(k) \in \mathbb{R}^{l_{y_0}}$ is the intercalation side current j_s, $u(k) \in \mathbb{R}^{l_u}$ is film resistance R_{SEI}, $w(k) \in \mathbb{R}^{l_w}$ is either I or V depending on cycle, and $k \geq 0$. Next,

$$u(k) = G(y_0(k)), \tag{16}$$

where $G(\cdot)$ is the unknown battery health submodel (9)-(12).

Next, we construct a model of the real system from the DFN model

$$\hat{x}(k+1) = f(\hat{x}(k)) + g_u(\hat{u}(k)) + g_{k,w}(w(k)), \tag{17}$$
$$\hat{y}(k) = h_k(\hat{x}(k)), \tag{18}$$
$$\hat{y}_0(k) = h_0(\hat{x}(k)), \tag{19}$$
$$z(k) = \hat{y}(k) - y(k), \tag{20}$$

where $\hat{x}(k) \in \mathbb{R}^n$, $\hat{y}(k) \in \mathbb{R}^{l_y}$, $z(k) \in \mathbb{R}^{l_z}$, $\hat{y}_0(k) \in \mathbb{R}^{l_{y_0}}$, $\hat{u}(k) \in \mathbb{R}^{l_u}$, and

$$\hat{u}(k) = \hat{G}(\hat{y}_0(k)), \tag{21}$$

where $\hat{G}(\cdot)$ is an estimate of $G(\cdot)$.

Next let A, B, D_1, and E_1 be the linear counterparts of f, g_u, $g_{k,w}$, and h_k and respectively. For $i \geq 1$, define the Markov parameter

$$H_i \triangleq E_1 A^{i-1} B. \tag{22}$$

Let r be a positive integer. Then, for all $k \geq r$,

$$\hat{x}(k) = A^r \hat{x}(k-r) + \sum_{i=1}^{r} A^{i-1} B \hat{u}(k-i) + \sum_{i=1}^{r} A^{i-1} D_1 w(k-i), \tag{23}$$

and thus

$$z(k) = E_1 A^r \hat{x}(k-r) + \sum_{i=1}^{r} E_1 A^{i-1} D_1 w(k-i) - y(k) + \bar{H}\bar{U}(k-1), \tag{24}$$

where

$$\bar{H} \triangleq \begin{bmatrix} H_1 & \cdots & H_r \end{bmatrix} \in \mathbb{R}^{l_z \times r l_u}$$

and

$$\bar{U}(k-1) \triangleq \begin{bmatrix} \hat{u}^{\mathrm{T}}(k-1) & \cdots & \hat{u}^{\mathrm{T}}(k-r) \end{bmatrix}^{\mathrm{T}}.$$

Next, we rearrange the columns of $\bar{H}$ and the components of $\bar{U}(k-1)$ and partition the resulting matrix and vector so that

$$\bar{H}\bar{U}(k-1) = \mathcal{H}' U'(k-1) + \mathcal{H} U(k-1), \tag{25}$$

where $\mathcal{H}' \in \mathbb{R}^{l_z \times (r l_u - l_U)}$, $\mathcal{H} \in \mathbb{R}^{l_z \times l_U}$, $U'(k-1) \in \mathbb{R}^{r l_u - l_U}$, and $U(k-1) \in \mathbb{R}^{l_U}$. Then, we can rewrite (24) as

$$z(k) = \mathcal{S}(k) + \mathcal{H} U(k-1), \tag{26}$$

where

$$\mathcal{S}(k) \triangleq E_1 A^r \hat{x}(k-r) + \sum_{i=1}^{r} E_1 A^{i-1} D_1 w(k-i) - y(k) + \mathcal{H}' U'(k-1). \tag{27}$$

Next, we rewrite (26) with a delay of k_j time steps, where $0 \le k_1 \le k_2 \le \cdots \le k_s$, in the form

$$z(k-k_j) = \mathcal{S}_j(k-k_j) + \mathcal{H}_j U_j(k-k_j-1), \tag{28}$$

where (27) becomes

$$\begin{aligned}\mathcal{S}_j(k-k_j) \triangleq{}& E_1 A^r \hat{x}(k-k_j-r) \\ &+ \sum_{i=1}^{r} E_1 A^{i-1} D_1 w(k-k_j-i) \\ &- y(k-k_j) + \mathcal{H}_j' U_j'(k-k_j-1)\end{aligned}$$

and (25) becomes

$$\begin{aligned}\bar{H}\bar{U}(k-k_j-1) = {}& \mathcal{H}_j' U_j'(k-k_j-1) \\ &+ \mathcal{H}_j U_j(k-k_j-1),\end{aligned} \tag{29}$$

where $\mathcal{H}_j' \in \mathbb{R}^{l_z \times (rl_u - l_{U_j})}$, $\mathcal{H}_j \in \mathbb{R}^{l_z \times l_{U_j}}$, $U_j'(k-k_j-1) \in \mathbb{R}^{rl_u - l_{U_j}}$, and $U_j(k-k_j-1) \in \mathbb{R}^{l_{U_j}}$. Now, by stacking $z(k-k_1), \ldots, z(k-k_s)$, we define the *extended performance*

$$Z(k) \triangleq \left[z^{\mathrm{T}}(k-k_1) \ \cdots \ z^{\mathrm{T}}(k-k_s)\right]^{\mathrm{T}} \in \mathbb{R}^{sl_z}. \tag{30}$$

Therefore,

$$Z(k) \triangleq \tilde{\mathcal{S}}(k) + \tilde{\mathcal{H}}\tilde{U}(k-1), \tag{31}$$

where

$$\tilde{\mathcal{S}}(k) \triangleq [\mathcal{S}(k-k_1) \ \cdots \ \mathcal{S}(k-k_s)]^{\mathrm{T}} \in \mathbb{R}^{sl_z}, \tag{32}$$

$\tilde{\mathcal{H}} \in \mathbb{R}^{sl_z \times l_{\tilde{U}}}$, and $\tilde{U}(k-1) \in \mathbb{R}^{l_{\tilde{U}}}$. The vector $\tilde{U}(k-1)$ is formed by stacking $U_1(k-k_1-1), \ldots, U_s(k-k_s-1)$ and removing repetitions of components. The coefficient matrix $\tilde{\mathcal{H}}$ consists of the entries of $\mathcal{H}_1, \ldots, \mathcal{H}_s$ arranged according to the structure of $\tilde{U}(k-1)$. Furthermore, we assume that the last entry of $\tilde{U}(k-1)$ is a component of $\hat{u}(k-r)$.

Next, we define the *surrogate performance*

$$z(k-k_j)^* \triangleq \mathcal{S}_j(k-k_j) + \mathcal{H}_j U_j^*(k-k_j-1), \tag{33}$$

where the actual past subsystem outputs $U_j(k-k_j-1)$ in (28) are replaced by the surrogate subsystem outputs $\hat{U}_j^*(k-k_j-1)$. The *extended surrogate performance* for (33), which is defined as

$$Z^*(k) \triangleq \left[z^{*\mathrm{T}}(k-k_1) \ \cdots \ z^{*\mathrm{T}}(k-k_s)\right]^{\mathrm{T}} \in \mathbb{R}^{sl_z}, \tag{34}$$

is given by

$$Z^*(k) = \tilde{\mathcal{S}}(k) + \tilde{\mathcal{H}}\tilde{U}^*(k-1), \tag{35}$$

where the components of $\tilde{U}^*(k-1) \in \mathbb{R}^{l_{\tilde{U}^*}}$ are components of $\hat{U}_1^*(k-k_1-1), \ldots, \hat{U}_s^*(k-k_s-1)$ ordered in the same way as the components of $\tilde{U}^*(k-1)$. Subtracting (31) from (35) yields

$$Z^*(k) = Z(k) - \tilde{\mathcal{H}}\tilde{U}(k-1) + \tilde{\mathcal{H}}\tilde{U}^*(k-1). \tag{36}$$

Finally, we define the *retrospective cost function*

$$\begin{aligned}\bar{J}(\tilde{U}^*(k-1),k) \triangleq{}& Z^{*\mathrm{T}}(k) R(k) Z^*(k) \\ &+ \eta(k)\tilde{U}^{*\mathrm{T}}(k-1)\tilde{U}^*(k-1),\end{aligned} \tag{37}$$

where $R(k) \in \mathbb{R}^{l_z s \times l_z s}$ is a positive-definite performance weighting and $\eta(k) \ge 0$. The goal is to determine refined subsystem outputs $\hat{\tilde{U}}(k-1)$ that would have provided better performance than the subsystem outputs $U(k)$ that were applied to the system. The refined subsystem output values $\hat{\tilde{U}}(k-1)$ are subsequently used to update the subsystem estimate.

Substituting (36) into (37) yields

$$\begin{aligned}\bar{J}(\tilde{U}^*(k-1),k) = {}& \tilde{U}^*(k-1)^{\mathrm{T}} \mathcal{A}(k) \tilde{U}^*(k-1) \\ &+ \tilde{U}^{*\mathrm{T}}(k-1)\mathcal{B}^{\mathrm{T}}(k) + \mathcal{C}(k),\end{aligned} \tag{38}$$

where

$$\mathcal{A}(k) \triangleq \tilde{\mathcal{H}}^{\mathrm{T}} R(k) \tilde{\mathcal{H}} + \eta(k) I_{l_{\tilde{U}}}, \tag{39}$$

$$\mathcal{B}(k) \triangleq 2\tilde{\mathcal{H}}^{\mathrm{T}} R(k)[Z(k) - \tilde{\mathcal{H}}\tilde{U}(k-1)], \tag{40}$$

$$\begin{aligned}\mathcal{C}(k) \triangleq{}& Z^{\mathrm{T}}(k) R(k) Z(k) - 2Z^{\mathrm{T}}(k) R(k) \tilde{\mathcal{H}}\tilde{U}(k-1) \\ &+ \tilde{U}^{\mathrm{T}}(k-1)\tilde{\mathcal{H}}^{\mathrm{T}} R(k) \tilde{\mathcal{H}}\tilde{U}(k-1).\end{aligned} \tag{41}$$

If either $\tilde{\mathcal{H}}$ has full column rank or $\eta(k) > 0$, then $\mathcal{A}(k)$ is positive definite. In this case, $\bar{J}(\tilde{U}^*(k-1),k)$ has the unique global minimizer

$$\tilde{U}^*(k-1) = -\frac{1}{2}\mathcal{A}^{-1}(k)\mathcal{B}(k). \tag{42}$$

Subsystem Modeling

The estimated subsystem output $\hat{u}(k)$ is given by the exactly proper time-series model of order n_c given by

$$\hat{u}(k) = \sum_{i=1}^{n_c} M_i(k)\hat{u}(k-i) + \sum_{i=0}^{n_c-1} N_i(k)\hat{y}_0(k-i), \qquad (43)$$

where, for all $i = 1,\ldots,n_c$, $M_i(k) \in \mathbb{R}^{l_u \times l_u}$ and $N_i(k) \in \mathbb{R}^{l_u \times l_{\bar{y}_0}}$. The subsystem output (43) can be expressed as

$$\hat{u}(k) = \theta(k)\phi(k-1), \qquad (44)$$

where $\theta(k) \in \mathbb{R}^{l_u \times n_c(l_u + l_{y_0})}$, is

$$\theta(k) \triangleq [M_1(k) \ \cdots \ M_{n_c}(k) \ N_1(k) \ \cdots \ N_{n_c}(k)] \qquad (45)$$

and $\phi(k-1) \in \mathbb{R}^{n_c(l_u+l_{\bar{y}})}$,

$$\phi(k-1) \triangleq \big[\hat{u}^{\mathrm{T}}(k-1) \ \cdots \ \hat{u}^{\mathrm{T}}(k-n_c) \ \hat{y}_0^{\mathrm{T}}(k-1) \ \cdots \ \hat{y}_0^{\mathrm{T}}(k-n_c)\big]^{\mathrm{T}}. \qquad (46)$$

Recursive Least Squares Update

Led d be a positive integer such that $\tilde{U}^*(k-1)$ contains $u^*(k-d)$. We define the cumulative cost function

$$J_{\mathrm{R}}(\theta(k)) \triangleq \sum_{i=d+1}^{k} \lambda^{k-i} \| \phi^{\mathrm{T}}(i-d-1)\theta^{\mathrm{T}}(k) - u^{*\mathrm{T}}(i-d)\|^2 + \lambda^k(\theta(k)-\theta(0))P^{-1}(0)(\theta(k)-\theta(0))^{\mathrm{T}}, \qquad (47)$$

where $\phi(k-d)$ is given by (46) and $\lambda \in (0,1]$ is the forgetting factor. Minimizing (47) yields

$$\theta^{\mathrm{T}}(k) = \alpha(k)\theta^{\mathrm{T}}(0) + [1-\alpha(k)][\theta^{\mathrm{T}}(k-1) + P(k-1) \cdot \phi(k-d-1)[\phi^{\mathrm{T}}(k-d-1)P(k-1)\phi(k-d-1) + \lambda]^{-1}(\hat{u}(k-d) - \phi^{\mathrm{T}}(k-d-1)\theta^{\mathrm{T}}(k-1))]. \qquad (48)$$

The error covariance is updated by

$$P(k) = \alpha(k)P(0) + [1-\alpha(k)][\lambda^{-1}(k)P(k-1) - \lambda^{-1}(k)P(k-1)\phi(k-d-1) [\phi^{\mathrm{T}}(k-d-1)P(k-1)\phi(k-d-1) + \lambda(k)]^{-1} \qquad (49)$$

$$\cdot \phi^{\mathrm{T}}(k-d-1)P(k-1)], \qquad (50)$$

where $\alpha(k) \in (0,1)$ is an algorithm reset, that is, when $\alpha(k) = 1$ $\theta(k)$ and $P(k)$ are reset to their initial values. Furthermore we initialize the error covariance matrix as $P(0) = \beta I$, where $\beta > 0$.

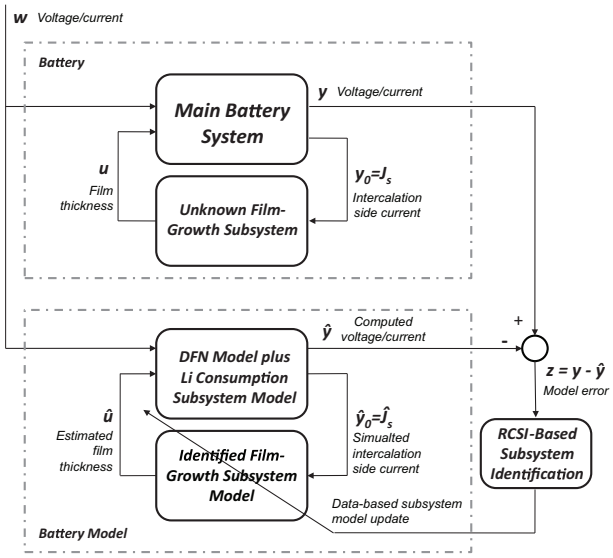

Figure 3. Specialization of Figure 1 to the film-growth identification problem.

NUMERICAL SIMULATION OF THE APPLICATION OF RCSI FOR FILM-GROWTH SUBSYSTEM IDENTIFICATION

We now present a numerical simulation of the application of RCSI to the film-growth identification problem. To this end, the DFN model together with the Li consumption component of the Ramadass battery-health model is considered as the Main System Model of the RCSI framework shown in Figure 1, and the film-growth component of the battery-health model is considered as the Unknown Subsystem to be identified. The adoption of this film-growth subsystem identification problem into the general RCSI framework is illustrated in Fig. 3. The Unknown Film-Growth Subsystem $G(\cdot)$ is connected to the Main Battery System $(f(\cdot), g_w(\cdot), g_u(\cdot), h(\cdot), h_0(\cdot))$ by feedback, which captures the fact that the film is driven by the intercalation side current, while the film impacts the local overpotential of the main reaction, restricting battery current. Note that neither the input $u(k)$ nor the output $y_0(k)$ of the film-growth subsystem is measured.

Although in practice the data, namely, battery terminal voltage and current, would be obtained from a physical experiment, the results in this section are based on simulations. To obtain simulated test data, the DFN+R battery model was simulated under repeated Constant-Current, Constant-Voltage (CCCV) cycling from 2 to 3.6 V at a 2.5 C-rate. The parameters for the DFN model are taken from (13). For the Ramadass health model the parameters are assumed to be $u_{sd,ref} = 0.4$, $i_{0s} = 4 \times 10^{-9}$, $M_p = 7.3 \times 10^4$, $\rho_p = 2.1 \times 10^3$, and $K_p = 1$. The film-growth subsystem was then removed from the truth model in accordance with the assumption that it is unknown. RCSI was then tasked with identifying the dynamics of the Unknown Film-Growth Subsystem. The controller and tuning parameters where chosen to be $n_c = 7$, $\eta(k) = 0$, $P(0) = 5 \times 10^{-7}$. In the absence of esti-

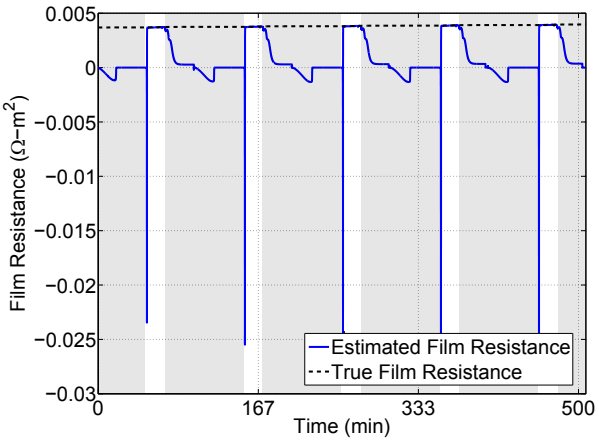

Figure 4. True film thickness and the film thickness as estimated by RCSI. Shaded regions indicate when the intercalation side current J_s is close to zero.

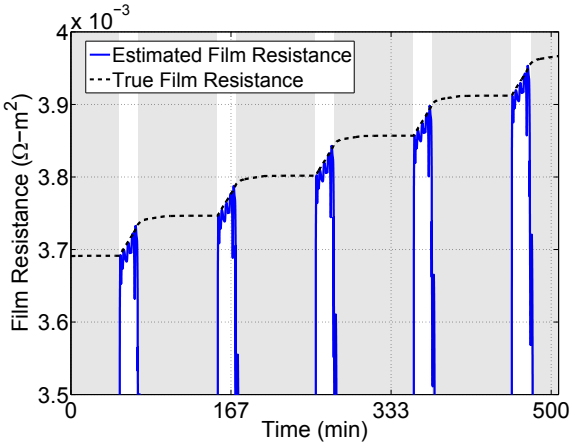

Figure 5. A magnified view of Figure 4.

mates of A, B, and E_1, we choose $\tilde{\mathcal{H}} = [\hat{H}_1]$, where $\hat{H}_1 = 0.01$. Next, $\hat{y}_0(k)$ is the intercalation side current J_s, and y is the system output voltage or current depending on the cycle. Finally, $\alpha(k) = 1$ at the start of each cycle, that is, $P(k)$ and $\theta(k)$ are re-initialized at the start of each charging cycle.

Figure 4 shows the true (that is, truth-model) film thickness as given by DFN+R model and the film thickness as estimated by RCSI. The film-thickness estimates show that the film-thickness subsystem dynamics are not identifiable during intervals of operation within which the intercalation side current J_s is close to zero. However, when J_s is large, RCSI produces a useful estimate of the film thickness that is close to the true film thickness. Figure 4 provides a magnified view of Fig. 4, which shows that the estimates of film thickness provided by RCSI correspond closely to the true film thickness during intervals in which J_s is large. The resulting identified film-growth model can be used to identify unknown physics, validate hypothesized physics, or predict the future behavior of the battery.

Figure 6 (a) shows the time history of θ, where θ are the coefficients of the estimated transfer function between the estimated intercalation side current and estimated film resistance. We note that θ is reset to zero at the start of each cycle. 6 (b) shows the normalized estimated intercalation side current and the normalized estimated film resistance. Since the process between intercalation side current and the estimated film resistance is modeled using transfer functions, when the input (intercalation side current) to the transfer function is approximately zero, the film resistance estimate will tend to zero, which means the estimates when the side current is small are unreliable.

Figure 7 (a) shows the pole-zero plot of the estimated subsystem at $t = 470$ mins. The estimated subsystem is approximately a finite impulse response (FIR) system, note the grouping of poles at the origin. Furthermore, Figure 7 (b) shows the impulse response of the subsystem, which supports the observation

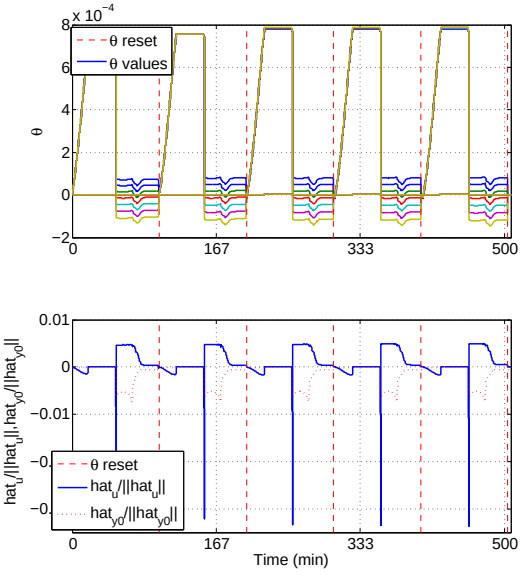

Figure 6. (a) is the time evolution of θ. These parameters are the coefficients of the transfer function from the estimated intercalation side current to the estimated film resistance. Note that θ is reset to zero at the start of each cycle. (b) is shows the normalized traces of estimated intercalation side current and estimated film resistance. When intercalation side current is near zero, the estimates of the film resistance tend to zero and are unreliable.

that the subsystem is approximately FIR.

RCSI AND FISHER INFORMATION

In the previous section it was discovered that the difference between the estimated film resistance and the true film resistance

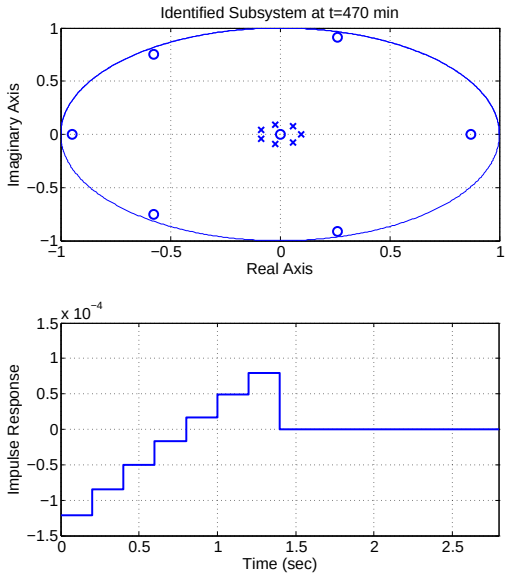

Figure 7. (a) is a pole-zero plot of the estimated transfer function from intercalation side current to film resistance at $t = 470$ min. Note that the transfer function is approximately a finite impulse response system, although an infinite-impulse response model structure is used for model refinement. (b) shows the impulse response of this transfer function.

was small during specific battery modes, namely, during charging when current is the input and voltage is the output. This suggests that the unknown subsystem is unidentifiable when voltage is the input and current is the output. We investigate this conjecture by considering three signals: battery current I, battery terminal voltage V, and the the local volumetric current density of the side reaction j_s. I and V are both inputs and outputs of the full model depending on whether the battery is in a constant current or constant voltage mode. j_s is the only input to the subsystem model. Two parameters are investigated: the initial condition of anode solid state electrolyte resistance R_{SEI_0} and the side reaction's exchange current density i_{0s}. Furthermore, R_{SEI_0} is related to R_{SEI} which is both a state and an output of the subsystem model; i_{0s} is the single parameter of then unknown subsystem. All six signal-parameter pairings are considered as possible predictors for when the difference between the estimated film resistance and the true film resistance will be small.

Fisher information is used to measure information carried by a signal about a parameter (14). In the single-parameter case the multiplicative inverse of Fisher information places a lower bound on the estimation variance for a specific parameter from a given signal; this follows directly from the Cramér-Rao bound, see (14). Specifically, we use Fisher Information Per Sample (FIPS), which has the form

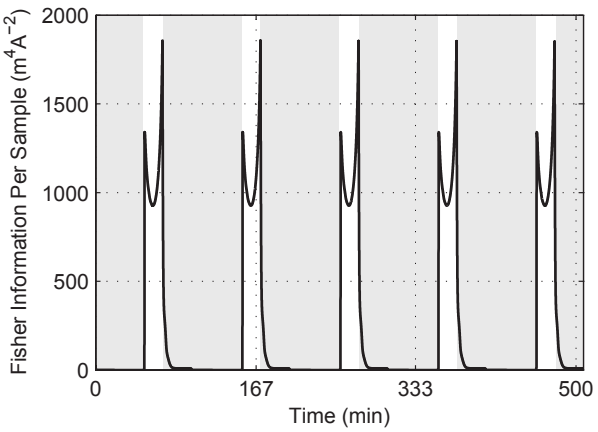

Figure 8. Fisher Information Per Sample of i_{0s} carried by j_s.

$$FIPS(k) \triangleq \frac{1}{\sigma^2}\left(\frac{\partial \xi(k)}{\partial \varphi}\right)^2, \tag{51a}$$

$$\xi \in \{I, V, j_s\}, \tag{51b}$$

$$\varphi \in \{R_{SEI_0}, i_{0s}\}, \tag{51c}$$

where k is the sample index, and σ^2 is the variance of the measurement signal, ξ is the signal carrying information about the parameter φ. The partial derivative is a measure of how the signal ξ is affected by infinitesimal perturbations of the parameter φ. In this numerical study the effects of noise on FIPS are removed by setting $\sigma^2 = 1$. Figure 8 is a plot of FIPS, specifically, information about i_{0s} carried by j_s. Larger values of FIPS indicate data steps when i_{0s} can be estimated more accurately using the signal j_s. Note that the FIPS peaks while in charging mode during which current is the input and voltage is the output, which is in agreement with the times at which RCSI accurately estimates the model. The remaining five parameter-signal pairings did not yield any useful correlation to the accuracy of the estimated film growth.

CONCLUSIONS AND FUTURE RESEARCH

As the first step of a noninvasive solution to battery-health diagnostics, we applied RCSI to the problem of estimating the SEI film-growth subsystem of a battery model for which the main system is the DFN model augmented with a Li consumption model. Assuming that the main system model is accurate and the measurements are noise free, RCSI was able to reproduce the output of the "truth" film-growth model when the intercalation side current J_s is not close to zero. Future research will focus on the case in which the DFN model is uncertain (that is, does not match the true battery characteristics) and the measurements are noisy. The ultimate goal is to apply the subsystem identification method to experimental battery data.

ACKNOWLEDGMENT

This work was supported by NASA GSRP grant NNX09AO55H and NSF grant 0835995.

REFERENCES

[1] Wang, J., Liu, P., Hicks-Garner, J., Sherman, E., Soukiazian, S., Verbrugge, M., Tataria, H., Musser, J., and Finamore, P., 2011. "Cycle-life model for graphite-lifepo4 cells". *J. Power Sources,* **196**, pp. A260–A271.

[2] Plett, G., 2004. "Extended kalman filtering for battery management systems of lipb-based hev battery packs; part 1. background". *J. Power Sources,* **134**, June, pp. 252–261.

[3] Plett, G., 2004. "Extended kalman filtering for battery management systems of lipb-based hev battery packs; part 2. modeling and identification". *J. Power Sources,* **134**, June, pp. 262–2276.

[4] Plett, G., 2004. "Extended kalman filtering for battery management systems of lipb-based hev battery packs; part 3. state and parameter estimation". *J. Power Sources,* **134**, June, pp. 277–292.

[5] Palanthandalam-Madapusi, H., Renk, E. L., and Bernstein, D. S., 2005. "Data-Based Model Refinement for Linear and Hammerstein Systems Using Subspace Identification and Adaptive Disturbance Rejection". In Proc. Conf. Contr. Appl., pp. 1630–1635.

[6] Santillo, M. A., D'Amato, A. M., and Bernstein, D. S., 2009. "System Identification Using a Retrospective Correction Filter for Adaptive Feedback Model Updating". In Proc. Amer. Contr. Conf., pp. 4392–4397.

[7] D'Amato, A. M., and Bernstein, D. S., 2009. "Linear Fractional Transformation Identification Using Retrospective Cost Optimization". In Proc. SYSID, pp. 450–455.

[8] Morozov, A. M., D'Amato, A. M., Ali, A., Ridley, A. J., and Bernstein, D. S., 2011. "Retrospective-Cost-Based Model Refinement for System Emulation and Subsystem Identification". In Proc. Conf. Dec. Contr.

[9] D'Amato, A. M., Ridley, A. J., and Bernstein, D. S., 2011. "Adaptive Model Refinement for the Ionosphere and Thermosphere". *Statistical Analysis and Data Mining,* **4**, pp. 446–458.

[10] Doyle, M., Fuller, T., and Newman, J., 1993. "Modeling of galvanostaic charge and discharge of the lithium/polymer/insertion cell". *J. Electrochemical Society,* **140**, June, pp. 1526–1533.

[11] Fuller, T., Doyle, M., and Newman, J., 1994. "Simulation and optimization of the dual lithium ion insertion cell". *J. Electrochemical Society,* **141**, January, pp. 1–10.

[12] Ramadass, P., Haran, B., Gomadam, P. M., White, R., and Popov, B. N., 2004. "Development of first principles capacity fade model for li-ion cells". *J. Electrochemical Society,* **151**(2), January, pp. A196–A203.

[13] Forman, J., Moura, S., Stein, J. L., and Fathy, H. K., 2011. "Genetic parameter identification of the doyle-fuller-newman model from experimental cycling of a lifepo4 battery". In Proc. American Control Conference, pp. 362–369.

[14] Cover, T., and Thomas, J. *Elements of information theory*. Wiley series in telecommunications.